This is a copy of the published version, or version of record, available on the publisher's website. This version does not track changes, errata, or withdrawals on the publisher's site.

Consequences of sp2–sp3 boron isomerization in supercooled liquid borates

O. L. G. Alderman, C. J. Benmore, and J. K. R. Weber

Published version information

Citation: OLG Alderman, CJ Benmore and JKR Weber. "Consequences of sp2–sp3 boron isomerization in supercooled liquid borates." Appl Phys Lett 117, no. 13 (2020): 131901.

DOI: 10.1063/5.0024457

This article may be downloaded for personal use only. Any other use requires prior permission of the author and AIP Publishing.

This version is made available in accordance with publisher policies. Please cite only the published version using the reference above. This is the citation assigned by the publisher at the time of issuing the APV. Please check the publisher's website for any updates.

This item was retrieved from **ePubs**, the Open Access archive of the Science and Technology Facilities Council, UK. Please contact epublications@stfc.ac.uk or go to http://epubs.stfc.ac.uk/ for further information and policies.

Applied Physics Letters

Consequences of sp^2–sp^3 boron isomerization in supercooled liquid borates

Cite as: Appl. Phys. Lett. **117**, 131901 (2020); https://doi.org/10.1063/5.0024457
Submitted: 07 August 2020 . Accepted: 09 September 2020 . Published Online: 28 September 2020

O. L. G. Alderman, C. J. Benmore, and J. K. R. Weber

COLLECTIONS

This paper was selected as Featured

View Online Export Citation CrossMark

ARTICLES YOU MAY BE INTERESTED IN

Toward quantum efficiency enhancement of kesterite nanostructured absorber: A prospective of carrier quantization effect
Applied Physics Letters **117**, 133901 (2020); https://doi.org/10.1063/5.0013504

Temporal acoustic wave computational metamaterials
Applied Physics Letters **117**, 131902 (2020); https://doi.org/10.1063/5.0018758

Electrostatic-doping-controlled phase separation in electron-doped manganites
Applied Physics Letters **117**, 132405 (2020); https://doi.org/10.1063/5.0024431

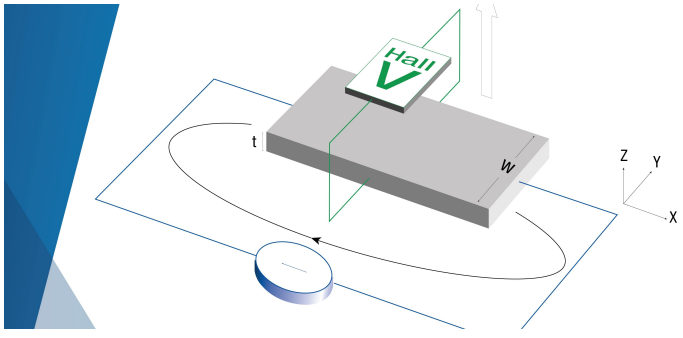

Tips for minimizing Hall measurement errors

Download the Technical Note

Lake Shore CRYOTRONICS

© 2020 Author(s).

Applied Physics Letters ARTICLE scitation.org/journal/apl

Consequences of sp^2–sp^3 boron isomerization in supercooled liquid borates

Cite as: Appl. Phys. Lett. **117**, 131901 (2020); doi: 10.1063/5.0024457
Submitted: 7 August 2020 · Accepted: 9 September 2020 ·
Published Online: 28 September 2020

View Online Export Citation CrossMark

O. L. G. Alderman,[1,a] C. J. Benmore,[2] and J. K. R. Weber[2,3]

AFFILIATIONS

[1]ISIS Neutron and Muon Source, Science and Technology Facilities Council, Rutherford Appleton Laboratory, Harwell Campus, Didcot OX11 0QX, United Kingdom
[2]X-ray Science Division, Advanced Photon Source, Argonne National Laboratory, Argonne, Illinois 60439, USA
[3]Materials Development, Inc., Arlington Heights, Illinois 60004, USA

[a]Author to whom correspondence should be addressed: oliver.alderman@stfc.ac.uk

ABSTRACT

Time-resolved high-energy synchrotron x-ray total scattering measurements on supercooled molten lithium metaborate ($LiBO_2$) reveal an isomerization reaction involving conversion of trigonal sp^2 boron to tetrahedral sp^3 boron during quenching and glass formation. Van't Hoff analysis yields an accurate enthalpy change, $\Delta H = 21(1)$ kJ mol^{-1} boron, from which we develop an analytical model for the sp^3 isomer fraction and its contribution to configurational heat capacity (C_p^{conf}) and entropy as a function of temperature and composition. Isomerization constitutes 40% of the total calorimetric C_p^{conf} at the glass transition for $LiBO_2$ and directly contributes to the observed rise in liquid fragility with the lithium content.

Published under license by AIP Publishing. https://doi.org/10.1063/5.0024457

The societal and fundamental importance of supercooled liquids cannot be overstated. They are the progenitor non-equilibrium state for all functional glasses, glass-ceramics, and crystals derived from the melt. They can be exploited directly as energy storage media[1] and in high-temperature sealing applications[2,3] and occur in many natural and industrial settings.[4] Despite tremendous progress in understanding the nature of supercooled liquids and the glass transition, connecting the structure to the associated dynamical arrest remains elusive, especially experimentally.[5]

Borates exhibit rich structural diversity stemming from the dependence of boron hybridization (sp^2 or sp^3) on pressure, temperature, and composition.[6] Herein, we show that borate liquids provide a rare insight into structural changes occurring during cooling and glass formation and that diffraction experiments can provide a means to directly quantify the structural contribution to configurational heat capacity (C_p^{conf}) and entropy (S^{conf}) loss during dynamical arrest.

Our experimental study focuses on lithium metaborate, $LiBO_2$, which has a high fragility index ($m \approx 77$)[7,8] and lithium ion conductivity.[9–11] Accurate measurements of the sp^3 isomer fraction, $N_4(T)$, as a function of temperature, T, allow parameterization of a simple thermodynamic model based on the Li^+ cation content per boron, $J = Li_2O/B_2O_3$, controlling the abundance of negatively charged trigonal sp^2 ($B\emptyset_2O^-$) and tetrahedral sp^3 ($B\emptyset_4^-$) isomers. We, thereby, obtain analytical expressions for the boron isomerization contribution to $C_p^{conf}(T,J)$ and $S^{conf}(T,J)$ and propose a simple model allowing quantification of its contribution to the observed rise in $C_p^{conf}(T_g,J)$ with J and semi-quantitative contribution to the associated rise in liquid fragility, $m(J)$, at the empirical glass transition temperatures $T_g(J)$ for $J \leq 1$. These results demonstrate the importance of borate liquids for developing our understanding of the role of structure in the glass transition and point toward strategies for the thermobaric engineering of Li^+ ion conducting electrolytes and battery materials.

The central observations underlying our work are illustrated in Fig. 1. The B–O bond length distribution is clearly resolved in our x-ray pair distribution functions (PDFs) and upon cooling shifts to longer distances, increases in area, and narrows only marginally. All three of these observations are consistent with an isomerization reaction involving a change in coordination and hybridization of boron as follows:

$$B\emptyset_4^- \rightleftharpoons B\emptyset_2O^-, \quad (1)$$

which is also illustrated in Fig. 1. Peak fitting to the PDFs, as described in the supplementary material, yields the mean B–O bond length as a function of temperature, Fig. 2(a). This declines steeply with increasing temperature, in contrast to its gradual thermal expansion observed in pure B_2O_3.[12] We have demonstrated previously[13,14] that mean B–O

Published under license by AIP Publishing

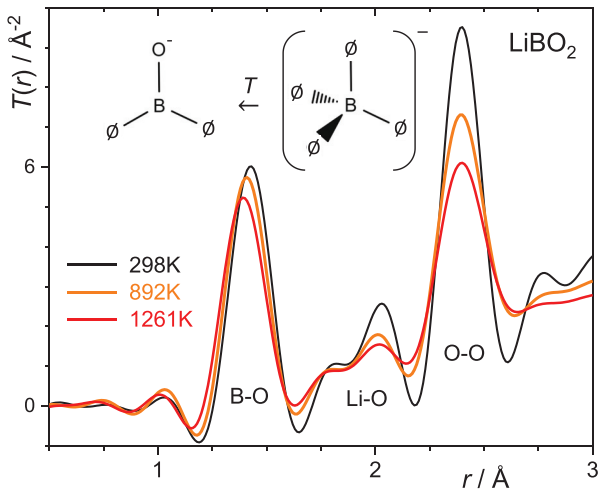

FIG. 1. Exemplary x-ray pair distribution functions for $LiBO_2$ liquid, supercooled liquid, and glass. The shift of the B–O peak to shorter distances at higher temperatures can be clearly discerned and is attributed to the $BØ_4^- \rightleftharpoons BØ_2O^-$ isomerization, schematic inset. Ø and O^- represent bridging and non-bridging oxygen bonded to two or one boron, respectively.

coordination numbers, n_{BO}, can be obtained accurately using bond length data, avoiding many of the systematic uncertainties affecting their direct determination from PDF peak areas. Figure 2(b) shows the results of using our bond-valence based approach, wherein a temperature-dependent bond-valence parameter accounts for thermal expansion due to vibrational anharmonicity. By construction, B_2O_3 has a constant n_{BO} of 3, whereas that for $LiBO_2$ rises continuously from ~3.1 above the melting point to ~3.4 below T_g. Both values are in excellent agreement with ^{11}B NMR[10,15,16] and non-resonant inelastic x-ray scattering[17] determinations for the glass and with both *ab-initio*[11] and classical[18] molecular dynamics models for the equilibrium liquid. Our time-resolved, diffraction-based data fill the gap between the ambient temperature measurements and the equilibrium liquid simulations. Assuming that chemical equilibrium is maintained for isomerization reaction 1, an accurate enthalpy of isomerization can be obtained by van't Hoff analysis, Fig. 3(a). The equilibrium constant is

$$K_1 = \frac{[BØ_2O^-]}{[BØ_4^-]} = \frac{J - N_4}{N_4} = \exp\left(-\frac{\Delta H}{RT} + \frac{\Delta S}{R}\right),\ 0 \le J \le 1, \quad (2)$$

where a unity activity coefficient ratio has been assumed. The total content of singly charged isomers is set by the Li^+ cation content per boron J. Therefore, the ratio of sp^2 metaborate anions to sp^3 boron is $(J - N_4)/N_4$. With boron present only as trigonal and tetrahedral species, it follows that $N_4 = n_{BO} - 3$, and thus K_1 can be computed directly from our diffraction derived n_{BO} in Fig. 2(b) and shown as a van't Hoff plot, Fig. 3(a). We, thereby, obtain an enthalpy change of 21(1) kJ mol^{-1} boron. This is in agreement with $\Delta H = 20(1)$ kJ mol^{-1} boron from an analogous analysis on our earlier x-ray diffraction data for supercooled sodium diborate liquid,[13,14] Fig. 3(a). Our ΔH values are a factor 1/3 of those determined by *in situ* Raman[19] and ^{11}B NMR[20] spectroscopies for a $Na_3B_7O_{12}$ liquid but in reasonable agreement with a revised ^{11}B NMR study[21] and estimates from *in situ* neutron diffraction[22] at a single temperature.

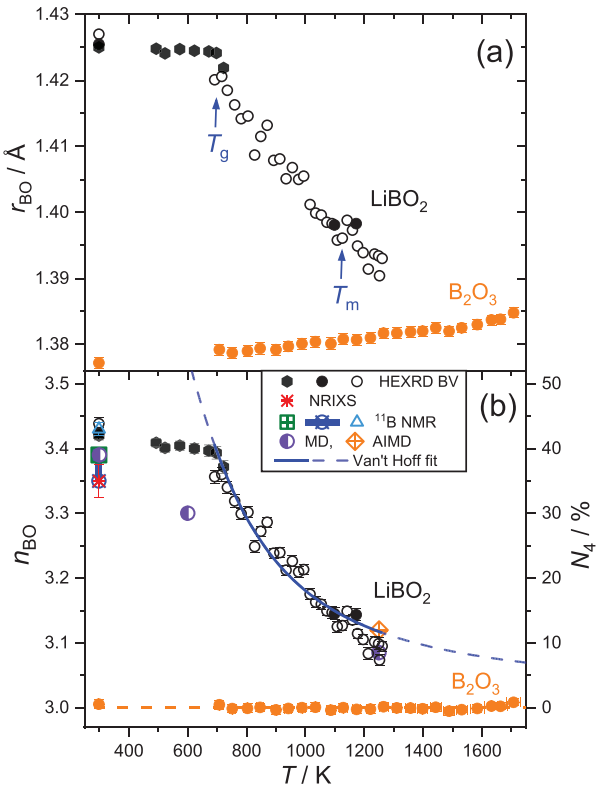

FIG. 2. Results of fitting to the B–O bond length distribution for $LiBO_2$ and B_2O_3.[12] (a) Mean B–O bond lengths, $r_{BO}(T)$. (b) Mean B–O coordination numbers, $n_{BO}(T)$, as derived from $r_{BO}(T)$ using the temperature-dependent bond-valence method.[13,14] For $LiBO_2$, open points correspond to 8s x-ray diffraction measurements during continuous cooling at −2.5(1) Ks^{-1}. Filled points correspond to 180 s isothermal measurements: liquid cooling (circles) or glass heating (hexagons). Comparison is made to literature data.[10,11,15–18] Glass transition and melting temperatures are indicated by arrows. The blue curve is the result of van't Hoff analysis (Fig. 3), with dashed extrapolation.

Rearranging Eq. (2), the analytical form for $n_{BO}(J,T)$ is

$$n_{BO}(J,T) = 3 + \frac{J}{1 + \exp\left(-\frac{\Delta H}{RT} + \frac{\Delta S}{R}\right)} = 3 + N_4,\ 0 \le J \le 1. \quad (3)$$

This is plotted in Fig. 2(b) for direct comparison to experimental data. However, plotting the equivalent curves for $N_4(J,T)$ over an extended temperature range, Fig. 3(b), it becomes clear why the isomerization transition is markedly more dramatic in molten $LiBO_2$ as compared to $Na_2B_4O_7$. The low temperature thermodynamic limit is $N_4(T \to 0) \to J$, while the high temperature limit is governed by ΔS. Thus, the larger alkali ion content in the metaborate and the apparently larger ΔS lead to a steeper transformation approaching T_g, where the isomerization reaction is arrested kinetically.

This behavior has direct consequences for the configurational heat capacity, with a contribution

$$C_P^{conf} = -\Delta H \frac{\partial N_4}{\partial T} = \frac{N_4}{J}\frac{\Delta H^2}{RT^2}(J - N_4). \quad (4)$$

Published under license by AIP Publishing

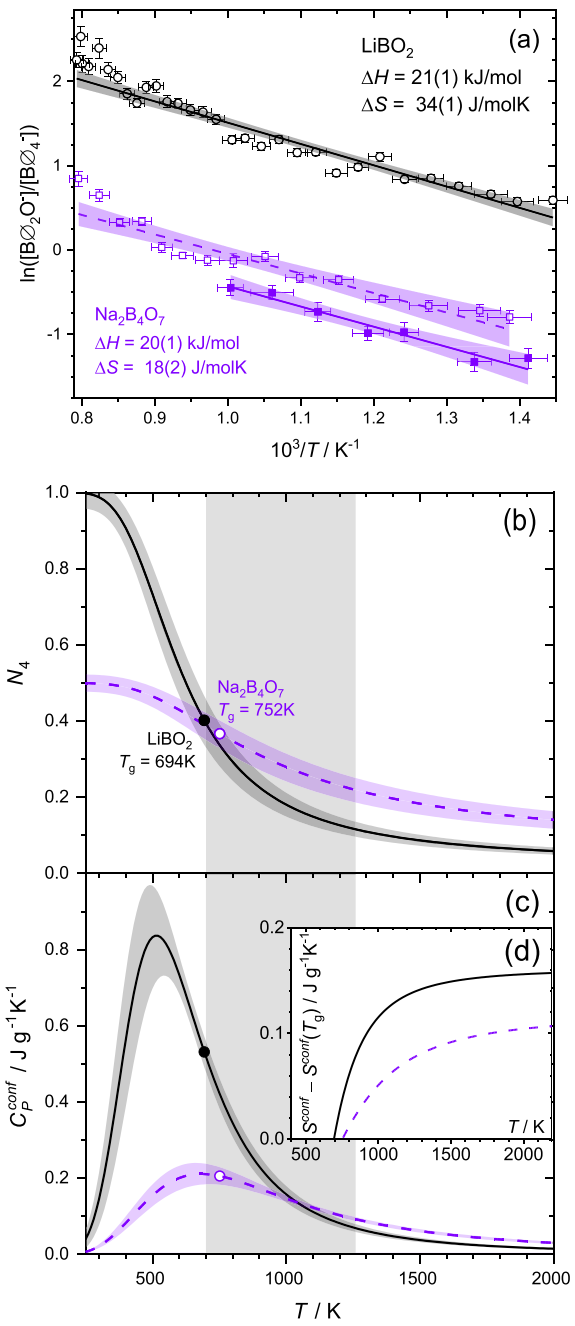

FIG. 3. (a) Van't Hoff plot for $B\emptyset_4^- \rightleftharpoons B\emptyset_2O^-$ equilibrium in liquid $LiBO_2$, based on data in Fig. 2(b), and for liquid $Na_2B_4O_7$ based on analogous x-ray diffraction data.[13,14] (b) Fraction of sp^3 boron, $N_4(T)$. Configurational (c) heat capacity and (d) entropy contributions. The shaded region represents the temperature range accessed by experiments. Points give the values at their respective T_g as indicated.

This is plotted in Fig. 3(c) for our two examples. It can be seen in Table I that the boron isomerization reaction accounts for about 25% of the total calorimetric C_p^{conf} at T_g in $Na_2B_4O_7$ and 40% in $LiBO_2$. This is similar to the 7%–30% range calculated from ^{11}B NMR data for alkali borosilicate[23] and aluminoborosilicate[24] glasses with varying fictive temperatures. Our results disagree with reports of the boron coordination change accounting for ~100% of $C_p^{conf}(T_g)$.[20,22] This is due to either uncertainties leading to overestimation of ΔH[20] or a missing factor of ΔN_4 in the calculation used.[22] Correcting the latter, we obtain contributions more consistent with our findings. However, any assessment of the contribution to $C_p^{conf}(T_g)$ based on the approximation

$$C_P^{conf}(T = T_g) \approx -\Delta H \frac{\Delta N_4}{\Delta T}, \tag{5}$$

will potentially be highly inaccurate where ΔT is large, as is the case for previous *in situ* studies based on only ambient glass and high-temperature liquid data.[20,22] Fictive temperature studies, where the ΔT range is close to T_g, can be much more accurate[23,24] but only where ΔN_4 is detectable. The latter stipulation depends on composition and measurement sensitivity and does not always hold.[21,25] Thus, our time-resolved *in situ* diffraction-based approach over wide temperature ranges, including the supercooled region, has clear advantages.

With a limited number of further assumptions, we can extend our simple model to explore its composition dependence ($0 \le J \le 1$). Based on our empirical findings, Fig. 3(a), we assume constant $\Delta H(J) = 21(1)$ kJ mol^{-1} boron and a linear $\Delta S(J) = J\Delta S(J=1)$. Then, using the empirical $T_g(J)$,[26,27] Fig. 4(a), we can calculate $N_4(T = T_g)$, which is in reasonable agreement with ambient ^{11}B NMR,[15] Fig. 4(b). The composition dependence of $C_p^{conf}(T = T_g)$ then follows from Eq. (4) and is shown in Fig. 4(c). It is apparent that the contribution of the boron isomerization reaction grows from zero at a low alkali content before rising continuously up to the metaborate composition. This behavior clearly contributes to, and even dominates, the observed rise in calorimetric $C_p^{conf}(T = T_g)$.[27] The remaining contributions to C_p^{conf} likely arise from small ring dissolution,[12,20,24,28] among other possibilities.

The temperature-dependent structural changes documented, thus far, have further implications for transport properties, including viscous flow. Adam and Gibbs[29] related the configurational entropy, $S^{conf}(T,J)$, to the temperature dependence of the viscosity,

$$\log_{10}\eta(T,J) = \log_{10}\eta_\infty + \frac{B(J)}{TS^{conf}(T,J)}. \tag{6}$$

TABLE I. Configurational heat capacities in supercooled liquid borates at their glass transition temperatures. Contributions of the $B\emptyset_4^- \rightleftharpoons B\emptyset_2O^-$ isomerization reaction, as compared to total calorimetric values. Final digit uncertainties are given in parentheses.

	$C_p^{conf}(T = T_g)$ (J g^{-1} K^{-1})		
Material	Boron isomerization	Calorimetric total	Boron isomerization % of total
$LiBO_2$	0.53(4)	1.367(3)[27]	39(3)
$Na_2B_4O_7$	0.21(2)	0.852(3)[27]	24(3)
		0.82(2)[42]	25(3)
		0.65[43]	32(4)

Published under license by AIP Publishing

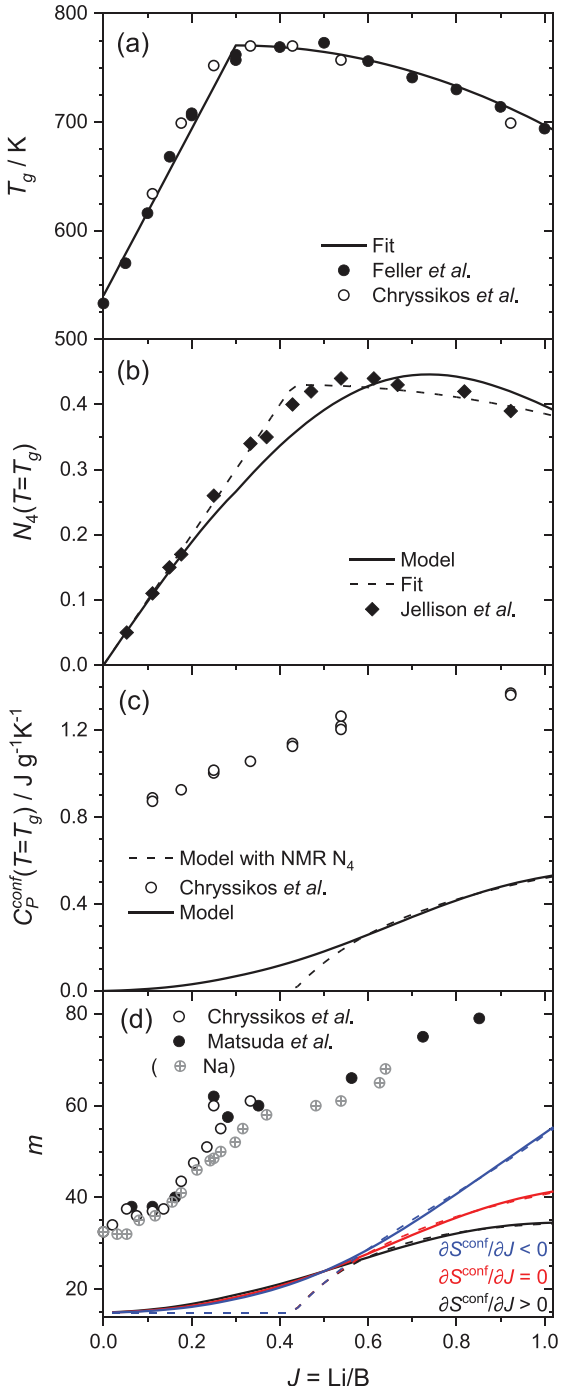

FIG. 4. Lithium borate (a) glass transition temperatures[26,27] with empirical fit. (b) $N_4(T_g)$ from Eq. (3), data in part a, constant $\Delta H(J) = 21(1)$ kJ mol^{-1} boron, and linearly varying $\Delta S(J) = J\Delta S(J=1)$, as compared to ambient ^{11}B NMR data.[15] An empirical fit is also shown. (c) Boron isomerization contributions to C_p^{conf} from Eq. (4) and each of the two curves in part b, as compared to calorimetric totals.[27] (d) Semi-quantitative contribution to the variation in the fragility index with composition. The results for three different assumptions for $S^{conf}(T_g)$ are shown, see the main text, and compared to the total fragilities from viscosity[27] and temperature-modulated DSC.[7]

S^{conf} is related to C_p^{conf} by[30]

$$S^{conf}(T,J) - S^{conf}(T=T_g,J) = \int_{T_g}^{T} \frac{C_P^{conf}(T',J)}{T'}\,dT' = \left[\frac{\Delta H}{T'}\{J - N_4(T',J)\} + JR\ln\left\{\frac{J}{N_4(T',J)}\right\}\right]_{T_g}^{T}, \quad (7)$$

where the second equality follows from evaluating the integral over Eq. (4) for the boron isomerization contribution to C_p^{conf}. Thus, the temperature-dependent part of S^{conf} rises with T, Fig. 3(d), leading to super-Arrhenius, or fragile, liquid behavior. The fragility index can be expressed in terms of $S^{conf}(T=T_g)$ and $C_p^{conf}(T=T_g)$,

$$m(J) \equiv \left.\frac{\partial \log_{10}\eta}{\partial(T_g/T)}\right|_{T=T_g} = m_0\left(1 + \frac{C_P^{conf}(T_g,J)}{S^{conf}(T_g,J)}\right), \quad (8)$$

based on Eq. (6), and with $m_0 = \log_{10}(\eta/\eta_\infty) \approx 14.9$, a constant.[31] While $S^{conf}(T=T_g,J)$ does not follow from our model, we can make a semi-quantitative analysis for the contribution of the boron isomerization reaction to the fragility index $m(J)$. Indeed, for constant $S^{conf}(T=T_g,J)$, $m(J)$ has the same functional form as $C_p^{conf}(T=T_g)$, as shown in Fig. 4(d) for a typical $S^{conf}(T=T_g,J) = 0.3$ J g^{-1} K^{-1}.[32,33] Two other cases are shown for $S^{conf}(T=T_g,J) = 0.2(1+J)$ and $0.2(2-J)$, i.e., with a positive or negative linear dependence on J. In all cases, it can be seen that $m(J)$ rises continuously up to $J=1$, as observed in the experimental fragilities, Fig. 4(d). A $\partial S^{conf}(T=T_g,J)/\partial J > 0$ is thought more likely given the fragility maximum *circa* $J=1$ indicated by temperature-modulated DSC data [Matsuda *et al.*,[7] data points at $[J, m] = [1.38, 71]$ and $[1.78, 66]$ are not shown in Fig. 4(d)]. It can also be seen in Fig. 4(d) that boron coordination change contributes little, or not at all, at low alkali contents, which is also reflected in the total experimental fragilities, varying little up to $J \approx 0.15$.

Lithium ion conductivity is known to decrease with the introduction of non-bridging oxygen[9,34,35] and, therefore, with a decrease in N_4 due to boron isomerization. Our findings are, therefore, consistent with the complex composition-temperature dependence measured in molten lithium borates.[9] In particular, the observed decrease in the temperature dependence of conductivity for Li_2O contents above 30 mol. % ($J = 0.43$) coincides with the increase in the temperature dependence of N_4, Fig. 4.

Our findings have consequences for the thermobaric engineering of borate material properties. Both applied pressure and sub-T_g relaxation (annealing) of lithium borate glasses are expected to lead to increases in N_4 and, thereby, Li^+ ion conductivity. This is due to the large enthalpic reservoir arising from $N_4 < J$. From the limited high-pressure studies available, it does indeed appear that the threshold pressure for the onset of the N_4 increase in alkali borates[36–38] is lower compared to that for pure B_2O_3.[39] Further studies on compression of $LiBO_2$ glass would be instructive.[36] Some studies[40,41] infer an opposite effect of annealing on N_4 to our model, and fictive temperature studies on $LiBO_2$ glasses should discriminate between these competing interpretations.

We have demonstrated that temperature-dependent boron-oxygen coordination numbers can be accurately derived from time-resolved high-energy x-ray diffraction, leading to accurate

Published under license by AIP Publishing

enthalpies, and estimates of entropies, of isomerization. We have derived an analytical model to calculate the contribution of sp^2–sp^3 isomerization to configurational heat capacities and entropies governing viscous flow. Further measurements would be beneficial for refining the composition dependence of our model. Nonetheless, we predict that thermobaric engineering of borate glass properties will be most effective around the metaborate composition, where the alkali ion content matches the boron content.

See the supplementary material for the complete experimental details and exemplary x-ray structure factors; PDF fitting procedure and exemplary plots; variation of the mean O–B–O angle with temperature inferred from fitting; variation of B–O and O–O PDF peak widths with temperature and comparison to pure B_2O_3; details of the isomerization model and limiting cases in the absence or completion of disproportionation; comparison to models with unspecified non-bridging oxygen atom association; effect of non-ideality; unit conversions for heat capacities and entropies; derivation of the expression for configurational entropy due to boron isomerization; details of the extension of the model to estimate composition dependence and fits to empirical glass transition temperatures and N_4 fractions; and numerical data for all experimental x-ray structure factors.

Emma Clark is gratefully acknowledged for assistance with sample synthesis and Anthony Tamalonis, Jessica Newhouse, and Jared Rafferty for assistance with beamline experiments.

This work was supported by the U.S. Department of Energy (DOE) under Grant Nos. SBIR DE-SC0015241 and DE-SC0018601 and NASA under Grant No. 80NSSC18K0059 (OLGA, RW). This research used resources of the Advanced Photon Source, a U.S. DOE Office of Science User Facility operated for the DOE Office of Science by Argonne National Laboratory under Contract No. DE-AC02-06CH11357.

DATA AVAILABILITY

The data that support the findings of this study are available within the article and its supplementary material.

REFERENCES

[1]A. Safari, R. Saidur, F. Sulaiman, Y. Xu, and J. Dong, Renewable Sust. Energy Rev. **70**, 905 (2017).
[2]R. K. Brow and D. R. Tallant, J. Non-Cryst. Solids **222**, 396 (1997).
[3]J. W. Fergus, J. Power Sources **147**(1), 46 (2005).
[4]P. G. Debenedetti and F. H. Stillinger, Nature **410**(6825), 259 (2001).
[5]C. P. Royall and S. R. Williams, Phys. Rep. **560**, 1 (2015).
[6]O. L. G. Alderman, Phys. Chem. Glasses **59**(1), 1 (2018).
[7]Y. Matsuda, Y. Fukawa, M. Kawashima, S. Mamiya, and S. Kojima, Solid State Ionics **179**(40), 2424 (2008).
[8]M. L. F. Nascimento and C. Aparicio, J. Phys. Chem. Solids **68**(1), 104 (2007).
[9]H. Fan, L. d Campo, V. Montouillout, and M. Malki, J. Non-Cryst. Solids **543**, 120160 (2020).
[10]V. Montouillout, H. Fan, L. del Campo, S. Ory, A. Rakhmatullin, F. Fayon, and M. Malki, J. Non-Cryst. Solids **484**, 57 (2018).
[11]T. Ohkubo, E. Tsuchida, M. Gobet, V. Sarou-Kanian, C. Bessada, and Y. Iwadate, J. Phys. Chem. B **117**(18), 5668 (2013).
[12]O. L. G. Alderman, G. Ferlat, A. Baroni, M. Salanne, M. Micoulaut, C. J. Benmore, A. Lin, A. Tamalonis, and J. K. R. Weber, J. Phys.: Condens. Matter **27**(45), 455104 (2015).
[13]O. L. G. Alderman, M. Liska, J. Machacek, C. J. Benmore, A. Lin, A. Tamalonis, and J. K. R. Weber, J. Phys. Chem. C **120**(1), 553 (2016).
[14]O. L. G. Alderman, C. J. Benmore, A. Lin, A. Tamalonis, and J. K. R. Weber, J. Am. Ceram. Soc. **101**(8), 3357 (2018).
[15]G. E. Jellison, S. A. Feller, and P. J. Bray, Phys. Chem. Glasses **19**(3), 52 (1978).
[16]Y. Yun and P. J. Bray, J. Non-Cryst. Solids **44**(2–3), 227 (1981).
[17]G. Lelong, L. Cormier, L. Hennet, F. Michel, J.-P. Rueff, J. M. Ablett, and G. Monaco, J. Non-Cryst. Solids **472**, 1 (2017).
[18]C. P. E. Varsamis, A. Vegiri, and E. I. Kamitsos, Phys. Rev. B **65**(10), 104203 (2002).
[19]T. Yano, N. Kunimine, S. Shibata, and M. Yamane, J. Non-Cryst. Solids **321**(3), 147 (2003).
[20]S. Sen, J. Non-Cryst. Solids **253**, 84 (1999).
[21]J. Wu, M. Potuzak, and J. F. Stebbins, J. Non-Cryst. Solids **357**(24), 3944 (2011).
[22]O. Majerus, L. Cormier, G. Calas, and B. Beuneu, Phys. Rev. B **67**(2), 024210 (2003).
[23]F. Angeli, O. Villain, S. Schuller, T. Charpentier, D. de Ligny, L. Bressel, and L. Wondraczek, Phys. Rev. B **85**(5), 054110 (2012).
[24]J. S. Wu and J. F. Stebbins, J. Non-Cryst. Solids **356**(41–42), 2097 (2010).
[25]J. F. Stebbins and S. E. Ellsworth, J. Am. Ceram. Soc. **79**(9), 2247 (1996).
[26]S. A. Feller, J. Kottke, J. Welter, S. Nijhawan, R. Boekenhauer, H. Zhang, D. Feil, C. Parameswar, K. Budhwani, and M. Affatigato, in *Proceedings of the Second International Conference on Borate Glasses, Crystals and Melts*, edited by A. C. Wright, S. A. Feller, and A. C. Hannon (DTIC Document, Sheffield, United Kingdom, 1997), p. 246.
[27]G. D. Chryssikos, J. A. Duffy, J. M. Hutchinson, M. D. Ingram, E. I. Kamitsos, and A. J. Pappin, J. Non-Cryst. Solids **172–174**, 378 (1994).
[28]J. F. Stebbins, Chem. Geol. **256**(3), 80 (2008).
[29]G. Adam and J. H. Gibbs, J. Chem. Phys. **43**(1), 139 (1965).
[30]A. Sipp, D. R. Neuville, and P. Richet, J. Non-Cryst. Solids **211**(3), 281 (1997).
[31]Q. Zheng and J. C. Mauro, J. Am. Ceram. Soc. **100**(1), 6 (2017).
[32]P. Richet, Geochim. Cosmochim. Acta **48**(3), 471 (1984).
[33]P. Richet, M. A. Bouhifd, P. Courtial, and C. Téqui, J. Non-Cryst. Solids **211**(3), 271 (1997).
[34]E. Hirose, K. Kataoka, H. Nagata, J. Akimoto, T. Sasaki, K. Niwa, and M. Hasegawa, J. Solid State Chem. **274**, 100 (2019).
[35]S. Ross, A.-M. Welsch, and H. Behrens, Phys. Chem. Chem. Phys. **17**(1), 465 (2015).
[36]L. Lei, D. He, K. He, J. Qin, and S. Wang, J. Solid State Chem. **182**(11), 3041 (2009).
[37]S. K. Lee, P. J. Eng, H-k Mao, Y. Meng, and J. Shu, Phys. Rev. Lett. **98**(10), 105502 (2007).
[38]S. K. Lee, P. J. Eng, H-k Mao, and J. Shu, Phys. Rev. B **78**(21), 214203 (2008).
[39]A. Zeidler, K. Wezka, D. A. J. Whittaker, P. S. Salmon, A. Baroni, S. Klotz, H. E. Fischer, M. C. Wilding, C. L. Bull, M. G. Tucker, M. Salanne, G. Ferlat, and M. Micoulaut, Phys. Rev. B **90**(2), 024206 (2014).
[40]M. S. Bødker, J. C. Mauro, R. E. Youngman, and M. M. Smedskjaer, J. Phys. Chem. B **123**(5), 1206 (2019).
[41]A. C. Wright, Phys. Chem. Glasses **51**(1), 1 (2010); available at https://www.ingentaconnect.com/content/sgt/ejgst/2010/00000051/00000001/art00001.
[42]J. Wu and J. F. Stebbins, J. Am. Ceram. Soc. **97**(9), 2794 (2014).
[43]D. R. Uhlmann, A. G. Kolbeck, and D. L. De Witte, J. Non-Cryst. Solids **5**, 426 (1971).

Published under license by AIP Publishing